VORTEX WAKES OF OSCILLATING CIRCULAR CYLINDERS

HONJI, Hiroyuki
Research Institute for Applied Mechanics, Kyushu University

TANEDA, Sadatoshi
Research Institute for Applied Mechanics, Kyushu University

https://doi.org/10.5109/7168671

出版情報：Reports of Research Institute for Applied Mechanics. 16 (54), pp.211-222, 1968. 九州大学応用力学研究所
バージョン：
権利関係：

Reports of Research Institute for Applied Mechanics
Vol. XVI, No. 54, 1968

VORTEX WAKES OF OSCILLATING CIRCULAR CYLINDERS

By

Hiroyuki HONJI and Sadatoshi TANEDA

The arrangements of vortices in the wake behind a circular cylinder making transverse sinusoidal oscillations in a uniform water flow were investigated experimentally at the Reynolds number range between 70 and 163. The dimensionless amplitudes were 0.40, 0.67, 1.43, 2.28 and 3.80, and the dimensionless oscillation frequencies varied from 0.05 to 0.30. Flow patterns at various oscillation frequencies were photographed by using both the Hydrogen-bubble method and the condensed-milk method for flow visualization. Periods and phases of the wake vortex formation were measured. The drag on a cylinder making a self-excited oscillatory motion was also measured by using the balance method. The main findings in the present investigation are as follows; 1) By vibrating the cylinder laterally, it is possible to control the wake frequency over a range of roughly 30% below and 20% above the natural shedding frequency. 2) The constant phase of vortex formation is maintained over the locked-in region. 3) The block structure of the wake appears at the ends of the locked-in region. 4) When the dimensionless amplitude of the cylinder is larger than the order of unity, the strength of the vortices is not equall for the two rows and each individual vortex of the stronger row consists of two smaller vortices having opposite rotations. 5) The predominant shedding frequency of such a distorted vortex wake agrees with the driving frequency. 6) The drag on the freely oscillating circular cylinder is increased when the shedding frequency is locked in to the natural frequency of the cylinder.

List of symbols

U_0 : Mean flow velocity
d : Cylinder diameter
A : Transverse displacement (peak-to-peak amplitude)
T_c : Period of cylinder oscillation
T_v : Period of vortex shedding
T_k : Period of natural vortex shedding
f : Vortex shedding frequency for freely oscillating cylinder
R : Reynolds number ($= U_0 d/\nu$; ν is the kinematic viscosity.)
A/d : Dimensionless amplitude
S_c : Dimensionless frequency of cylinder oscillation ($= d/T_c U_0$)
S_v : Dimensionless vortex formation frequency ($= d/T_v U_0$)
S_k : Strouhal number for natural vortex shedding
ϕ : Phase of vortex formation
C_D : Drag coefficient ($= D/\frac{1}{2}\rho U_0 F$; D is the drag, ρ the water density and F the projected area of circular cylinder.)

1. Introduction

As is well known, two rows of vortices called Kármán vortex street are formed in the wake behind a stationary circular cylinder. This flow past the non-oscillating cylinder has been studied extensively from earlier times by many research workers. In recent years, however, the flow past an oscillating obstacle has become the center of wide interest. The authors carried out the drag measurement with an oscillating circular cylinder, and the results were reported in a previous paper [1]. However, the flow pattern of the wake has remained unknown. When a cylinder is oscillated laterally at a constant frequency in a uniform fluid flow, the vortex wake which is somewhat different from the Kármán vortex street appears. The experiment described in this paper was undertaken to reveal such vortex wake geometries.

Recently, Berger [2], Wehrmann [3], and Koopmann [4] have investigated experimentally the wake of the oscillating cylinder. The region in which the vortex shedding is controlled by the oscillatory motion of the cylinder has been revealed through their investigations. A brief sketch of historical aspects of the subject is found in Koopmann's paper [4].

When a dimensionless amplitude of the cylinder oscillation is sufficiently large or the cylinder is oscillated at a frequency fairly different from normal one, interesting vortex wakes are formed. For instance, one of the authors (S. Taneda [5]) pointed out in his previous paper that the symmetric vortex street appears when the driving frequency is reduced to one-half of the normal shedding one. In this experiment, the similar investigation was made over a wider range of the oscillation frequency which included the exterior regions of the locked-in region around the normal shedding frequency. The Reynolds numbers employed have ranged from 70 to 163, the dimensionless amplitudes A/d from 0.40 to 3.80 and the dimensionless frequencies S_c from 0.05 to 0.30. It is a controversial question whether or not the flow around the freely oscillating obstacle is identical with that around the obstacle which is forced to oscillate. Taking this into consideration, the drag measurement was carried out with a freely oscillating circular cylinder.

2. Experimental Methods

2-1 Apparatus for investigating the oscillating wake

The experiment was carried out by towing an oscillating test cylinder in a water tank filled with still water. The hydrogen-bubble method was used as a visualization technique of flows. In several cases, the condensed-milk method was also employed for the same purpose. The experimental apparatus consisted of a small water tank (30 cm × 30 cm × 200 cm), a carriage of the test cylinder and a hydrogen-bubble generator. Fig. 1 shows the side view of the apparatus for the case in which a 8 mm cinecamera was employed, and Photo. 1

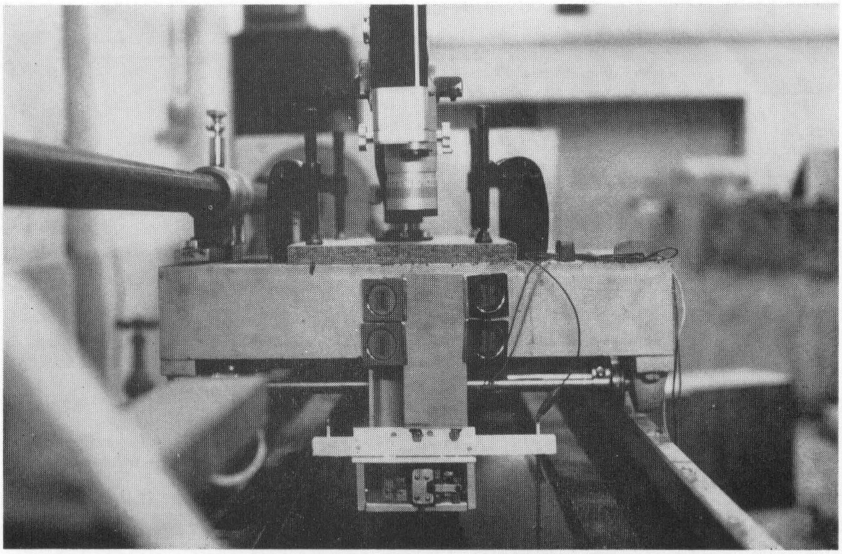

Photo. 1. Front view of the apparatus.

(*Facing p.* 212)

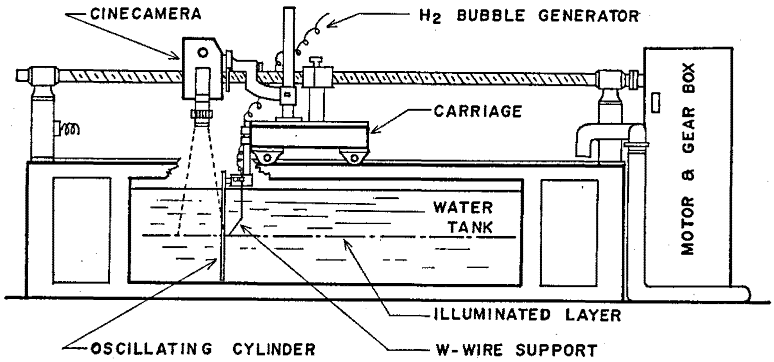

Fig. 1. Side view of the apparatus.

its front view. Vortex shedding frequencies were measured with a hot-wire anemometer. A shaker of the cylinder consisted of a small d-c motor, several reduction gears and a crank rod. Driving frequencies of the shaker were varied between 0.40 and 2.0 Hz by adjusting the out-put voltage of a stabilized d-c power supply. The test cylinders were made from well polished brass rods. The diameters of the cylinders were 0.30, 0.50 and 0.80 cm, and the under-water length of them was about 20 cm. The carriage velocities have ranged from 1.5 cm/s to 5.5 cm/s. The possible transverse displacements of the cylinder were 0.20 cm and 1.14 cm.

The techniques of flow visualization are described here in some detail. A fine straight tungsten wire (21 cm long and 50 $\mu\phi$ in diameter) which was stretched between two tips of the metal supports was used as the bubble generating wire. The wire was placed at a short distance about 0.5 cm ahead of the front surface of the cylinder. The most successful lighting was achieved when the incident light made an angle of about 65° with the cylinder axis. A 1 KW projector lamp was used as the light source. It is worth while nothing that when the bubble generating wire was placed upstream of the cylinder the wake-vortex centers appeared dark and their surroundings bright, on the other hand when it was placed downstream of the cylinder the vortex centers brightened and their surroundings became dark. The reason for this difference is not yet evident. The condensed-milk method was also used for the flow visualization. A cylinder was coated thinly with condensed milk, dried 2~3 minutes in air and towed in the water. Condensed milk melts in the water and makes streak lines visible.

Vortex formation periods were measured by using a hot-wire anemometer designed to be very sensitive to the change of flow direction. The distance between the probe-tip and the cylinder rear surface was 3.5 cm along the flow direction. The out-put signals from the hot-wire were recorded on the oscillograph papers. All the flow patterns presented in this report were photographed with a camera at rest with respect to the undisturbed water.

2-2 Apparatus for drag measurement

The whole arrangement is shown in Fig. 2. The uniform water flows were obtained by moving a glass water tank (30 cm × 30 cm × 90 cm). The drag force on a circular cylinder making self-excited oscillations was measured by means of the balance method. The test cylinder made from a brass rod was 26 cm in length, 0.5 cm in diameter and 44 gr in weight. It was suspended loosely by using low-friction pivots as shown in Fig. 3, so that it could oscillate freely about its horizontal axis. The natural frequency of this oscillating system was 1.03 Hz in still water. This pendulum system was further supported as a whole by two points and cups. The distance between the two points was 16 cm. In this way, the cylinder was allowed to swing only in a plane perpendicular to the flow, and the pendulum system in a plane parallel to the flow. The angle of inclination of the pendulum system in response to the drag acting on the under-water part of the cylinder was measured with the aid of the lamp and scale method. The observed deflection angle varied to a maximum of about 1/100. The drag and the shedding frequency measurements were made independently, since the hot-wire probe necessarily disturbed the wake.

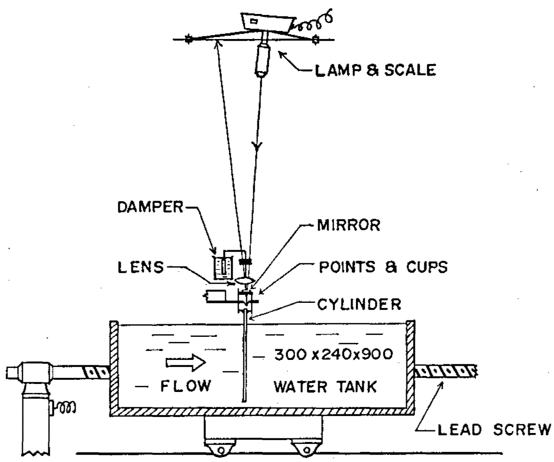

Fig. 2. Apparatus for measuring the drag.

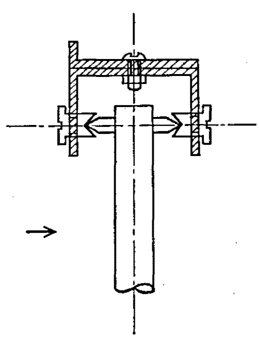

Fig. 3. Suspension of a test cylinder.

3. Experimental Results

3-1, Locked-in region

The resulting relationships between the dimensionless oscillation frequency and the dimensionless shedding frequency are shown in Figs. from 4 to 7. The dimensionless shedding frequency S_v depends on the Reynolds number R, the dimensionless frequency S_c, and the dimensionless amplitude A/d in the form,

$$S_v = f\ (R,\ S_c,\ A/d). \tag{1}$$

Figs. 4, 5 and 6 give the S_v/S_c vs. S_c relations at $R = 70$, 100 and 130 respectively. In each Figure, the horizontal dashed line corresponds to $S_v/S_c = 1$. All the measured S_v/S_c vs. S_c relationships have nearly the same general tendency. The intermediate region over which the dimensionless shedding frequency S_v is equall to the dimensionless oscillation frequency S_c is so called the locked-in region, where the vortex shedding is completely controlled by the oscillatory motion of the cylinder. An example of the S_v vs. S_c relation is shown in Fig. 7 for the case of $R = 100$. The horizontal and the vertical dashed lines indicate the corresponding Strouhal number S_k calculated from Roshko[6]'s empirical relation,

$$S_k = 0.212\ (1 - 21.2/R). \tag{2}$$

As is shown in Fig. 4, the shedding frequency was measured at $R = 70$ for the two cases of $A/d = 0.40$ and $A/d = 0.67$. From this figure, it can

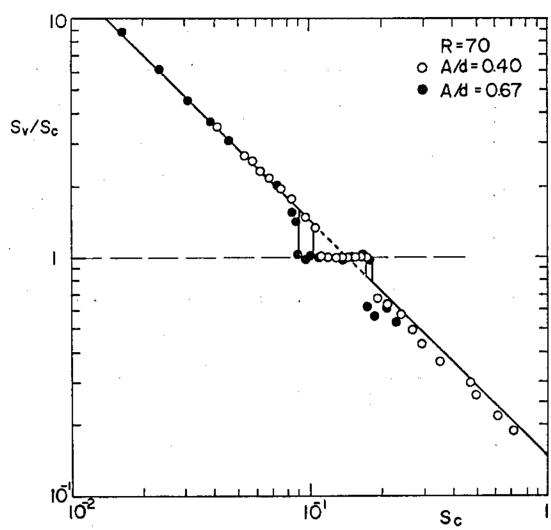

Fig. 4. S_v/S_c vs. S_c at R=70

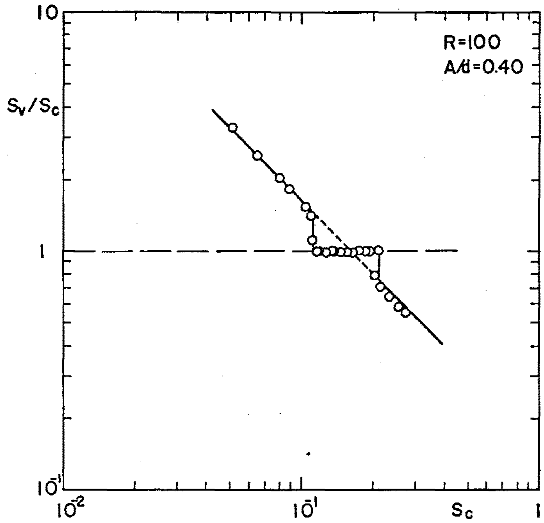

Fig. 5. S_v/S_c vs. S_c at R=100.

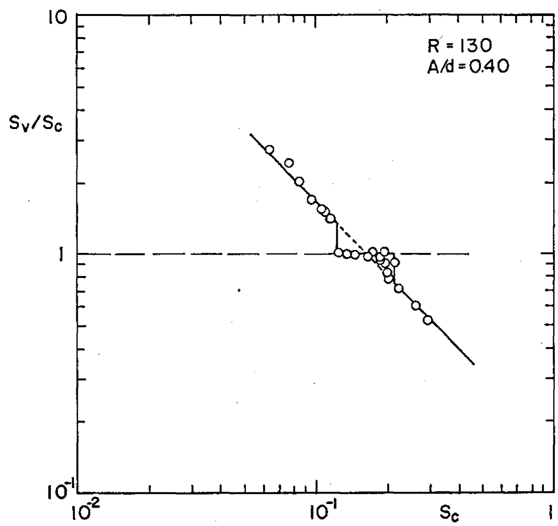

Fig. 6. S_v/S_c vs. S_c at R=130.

be seen that the range of locking-in increases with the dimensionless amplitude. This fact has been already pointed out by several investigators. The present results shown in Figs. 4, 5 and 6 indicate also that the oscillatory motion can control the frequency of the oscillating wake over a limited range of about 30 % below and 20 % above the normal shedding frequency. In any case, the

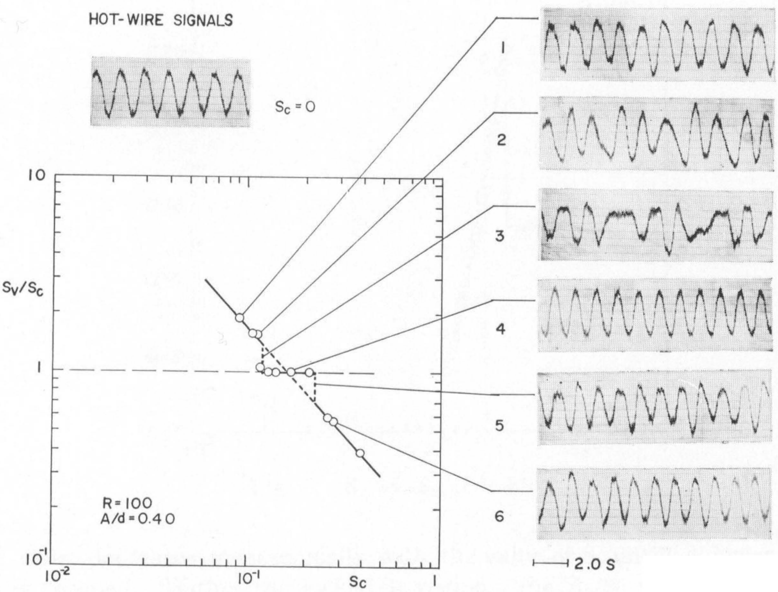

Photo. 2. Hot-wire signals

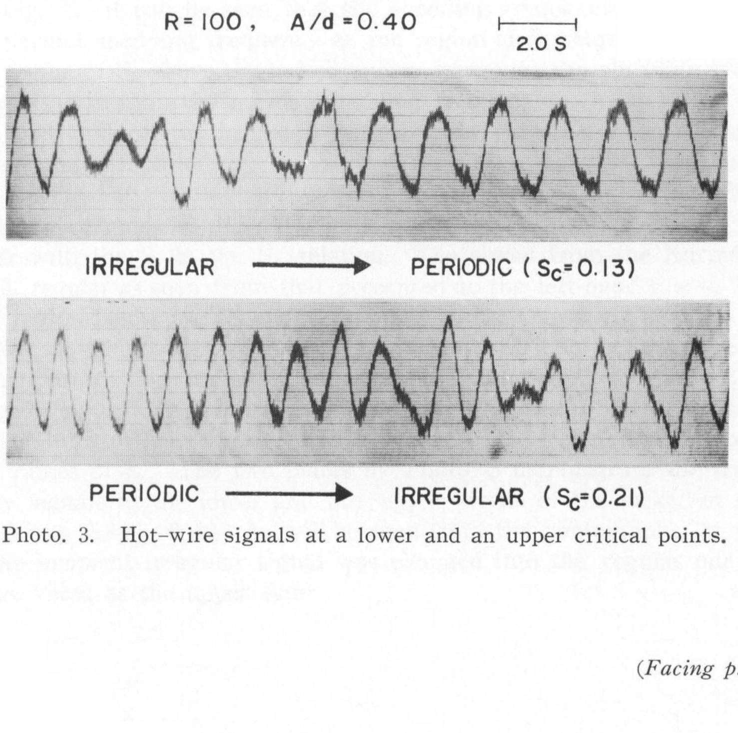

Photo. 3. Hot-wire signals at a lower and an upper critical points.

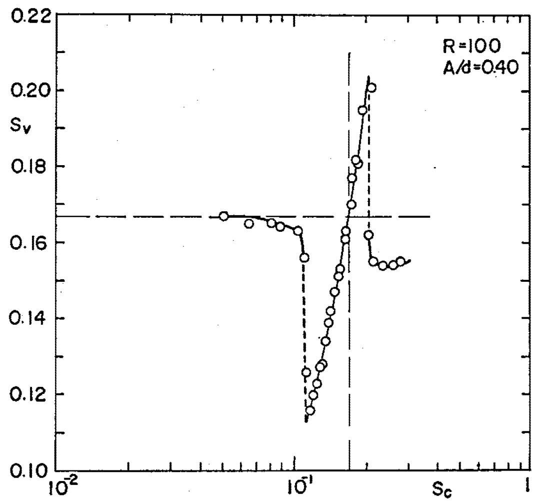

Fig. 7. S_v vs. S_c at R=100.

S_v/S_c value decreases monotonically with the value of S_c untill a lower critical limit is reached. Within the locked-in region, the S_v/S_c value is maintained constant. When an upper limit of the locked-in region is reached, the frequency lock-in is suddenly lost, and again S_v/S_c decreases with S_c monotonically. From Fig. 7, it can be seen that the shedding frequencies are nearly equall to the normal shedding frequency at the region of S_c below the locked-in one. At the region of S_c above the locked-in one, however, the shedding frequencies are slightly less than the normal shedding frequency.

At both ends of the locked-in region, flow patterns become unstable and irregular and the periodicity of vortex formation vanishes. It can be seen clearly by the hot-wire signal observation whether the wake is periodic or not. The hot-wire signals at $R = 100$ and $A/d = 0.40$ are displayed in Photo. 2 together with the S_v/S_c vs. S_c relation. The signal from the Kármán vortex street is regular as seen from that presented on the left-hand side in Photo. 2. At the region below the locked-in one, the signal shows yet a regular pattern as shown in Photo. 2-1. At the lower limit of the locked-in region, an irregular pattern appears as shown in Photos. 2-2 and 2-3. Photo. 2-4 shows the regular pattern in the locked-in region, Photo. 2-5 the irregular one at the upper limit of that region, and Photo. 2-6 the regular and stable one at higher values of S_c. The two plates of Photo. 3 demonstrate the transitional hot-wire signals at the lower and the upper limits of the locked-in region at $R = 100$ and $A/d = 0.40$. As will be seen from the photographs, at the lower limit the incipient irregular signal was changed into the regular one in time, and vice versa at the upper limit.

3-2 Phase of vortex formation

The result of the phase measurement in the locked-in region is presented. The phase ϕ is defined in the form

$$\phi = X/T_v U_0, \tag{3}$$

where X is the distance between the rear of the cylinder and the center of the vortex which is nearest to the cylinder, T_v the vortex formation period, and U_0 the uniform flow velocity (cf. Fig. 8). The value of $T_v U_0$ is approximately equall to the longitudinal spacing of the vortices. Fig. 9 shows the relationship between ϕ and S_c at $R = 100$ and $A/d = 0.40$. In order to indicate the corresponding locked-in region the relationship between S_v/S_c and S_c is shown in the same figure. From this figure, it can be seen that the measured phase is kept nearly constant ($\phi \sim 0.5$) all over the locked-in region. This

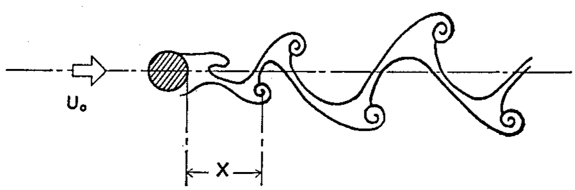

Fig. 8. Definition of X

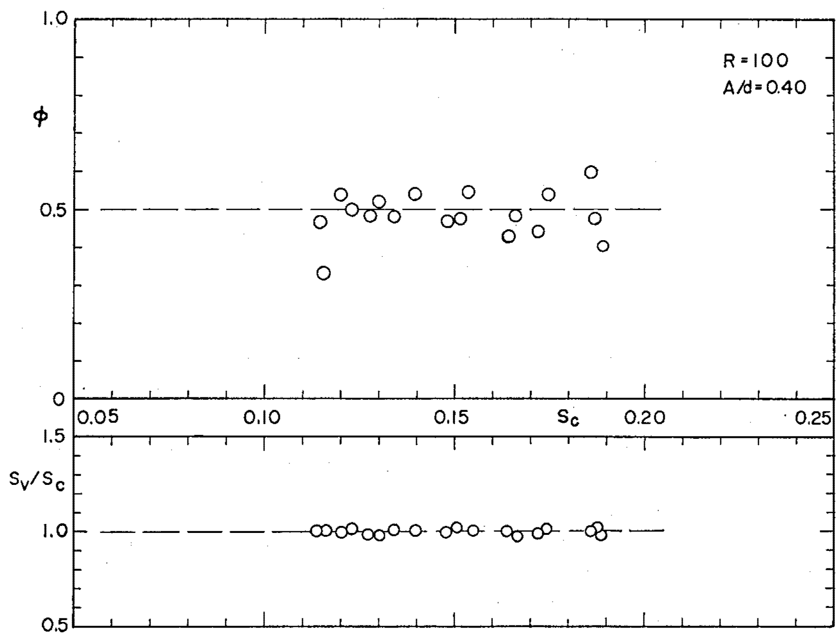

Fig. 9. ϕ and S_v/S_c vs. S_c at R=100.

means that the phase of vortex formation is independent of the oscillation frequency, although the longitudinal spacing of the consecutive vortices varies with the oscillation frequency in the locked-in region.

3-3 Flow patterns

The flow patterns are displayed in Photos. from 4 to 21. Fundamental data are given for each picture. The value of T_k is calculated from Eq. (2) and the relation,

$$S_k = d/T_k U_0. \tag{4}$$

Photos. from 4 to 9 show the flow patterns at $R = 100$ and $A/d = 0.40$. Photo. 4 shows the ordinary Kármán vortex street behind a stationary cylinder and Photo. 5 the flow pattern of a slowly oscillating cylinder at $T_c/T_k = 2.20$. Although the distances of two consecutive vortices in the flow direction are somewhat different from those of the Kármán vortex street, the regularity of the wake is still maintained completely. Photo. 6 shows the flow pattern at a lower limit of the locked-in region. It should be noted that there exists in the wake the block structure, which seems to be a phenomenon of beat resulting from a slight frequency difference between the oscillatory motion and the vortex shedding. Photo. 7 shows the flow pattern in which the shedding frequency is completely locked-in to the oscillation frequency. Photo. 8 shows the flow pattern at an upper limit of the locked-in region. Photo. 9 shows an example of the flow pattern visualized with the condensed-milk method. Photographs 10, 11 and 12 show the Kármán trail, the block structure of the wake, and the incipient stage of the frequency lock-in respectively at $R = 104$ and $A/d = 0.67$.

For the case in which the dimensionless amplitude A/d was larger than the order of unity, only the flow pattern observation was made in this experiment. The value of a shedding period T_v, however, can be estimated from the photograph of flow pattern by using the approximate relation,

$$T_v \sim L/U_0, \tag{5}$$

where L is the distance of consecutive vortices in the flow direction. Photos. from 13 to 16 show the flow patterns at $R = 104$ and $A/d = 2.28$. Photo. 13 shows the flow pattern behind a slowly oscillating cylinder at $T_c/T_k = 1.44$. When the dimensionless amplitude is larger than the order of unity, two rows of the vortices hold no longer the symmetric form, but the two rows seem to be different in the strength of the vortex. This fact was already pointed out by one of the authors (S. Taneda[7]). The more interesting property is that, as will be seen from Photo. 13, each individual vortex of one of the rows consists of two smaller vortices having opposite rotations. Another point of interest is that the inside vortices appear to be stronger than the outside ones. The value of T_v estimated from the photograph is about 2.1s and nearly equall to the measured value of T_c. This means that the predominant frequency of such a distorted vortex wake is still controlled by the driving frequency of the cylinder.

As will be seen from Photo. 14, when T_c/T_k is small the lateral spacing between the two rows increases remarkably far downstream. The estimated value of T_v is about 1.40 s, which is nearly equall to the measured value of T_c. This indicates that the vortex wake in this case is also locked-in. Photo. 15 shows the flow pattern at a slightly larger value of S_c. It will be seen that the distances between two consecutive vortices are fairly reduced. From the photograph the value of T_v is estimated to be about 1.2 s, which is nearly equall to the measured value of T_c. This shows that the wake is still locked-in. Photo. 16 shows the flow pattern for the large values of R and A/d, and Photo. 17 that for the large oscillation frequency. From these photographs, it can be seen that the vortices generated are splashed outside the turbulent wake.

Photos. from 18 to 21 show the flow patterns at $R = 95$ and $A/d = 3.80$. The vortex wake behind a slowly oscillating cylinder shows a regular sinusoidal form (Photo. 18). Photos. 19 and 20 show the successive flow patterns at $S_c = 0.049$. These pictures demonstrate that the vortices interact each other and the wake rearrange itself again into the configuration of the Kármán vortex street.

As will also be seen from Photos. 16, 17 and 20, the Kármán vortex street seems to have the general property of amplifying the external disturbances with the periods longer than its proper one. As was described in the previous papers [5)7)8)], the position where the disturbances are most amplified moves downstream as the period of the disturbances is increased. Therefore, the original Kármán vortex street collapses at some distance downstream, and finally only the vortex wake due to the external disturbances having the longer period survives and becomes dominant.

Photo. 21 shows the flow pattern at $S_c = 0.144$. In this case, the value of T_v is estimated to be about 1.40 s, which is two times that of T_c. This indicates that the locked-in frequency is not independent of the dimensionless amplitude, the role of which is not yet well understood. The block structure of the wake was not observed when the dimensionless amplitude was larger than the order of unity. Photographs from 4 to 12, except Photo. 9, were taken by using the hydrogen-bubble method, and Photographs from 13 to 21 the condensed-milk method.

3-4 Drag on a freely oscillating cylinder

The experimental result is shown in Fig. 10, in which the drag coefficient C_D and the shedding frequency f are plotted against the Reynolds number R. From this figure, it can be seen that the drag coefficient is slightly increased when the vortex wake is locked-in around $R = 130$. Fig. 11 shows a comparison of the drag coefficients between the two cases of forced and free oscillations. The drag coefficients for the forced oscillation at $S_c = 0.163$ are

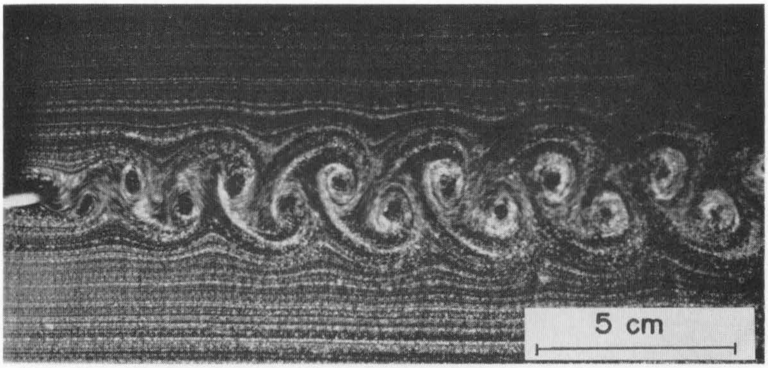

Photo. 4. Kármán vortex street behind a non-oscillating circular cylinder. ($R=100$, $A/d=0.40$, $S_c=0$, $S_v=0.158$; $U_o=2.45$ cm/s, $d=0.50$ cm)

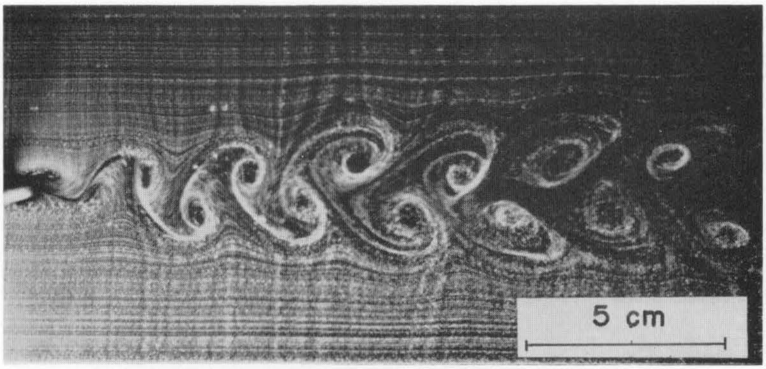

Photo. 5. Vortex wake behind a slowly oscillating cylinder. ($R=100$, $A/d=0.40$, $S_c=0.076$, $S_v=0.171$, $T_c/T_k=2.20$; $U_o=2.45$ cm/s, $d=0.50$ cm, $T_c=2.68$ s)

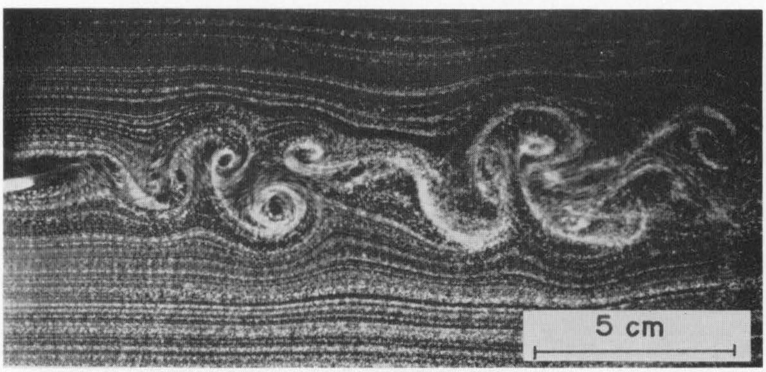

Photo. 6. Block structure of the vortex wake at a lower limit of the locked-in region. ($R=100$, $A/d=0.40$, $S=0.122$; $U_o=2.45$ cm/s, $d=0.50$ cm, $T_c=1.66$ s)

(*Facing p.* 220)

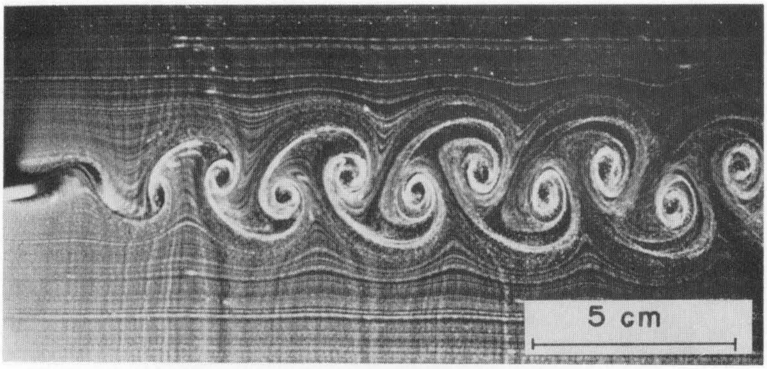

Photo. 7. Vortex wake which is locked completely.
($R=100$, $A/d=0.40$, $S_c=0.136$, $S_v=0.135$, $T_c/T_k=1.23$; $U_o=2.48$ cm/s, $d=0.50$ cm, $T_c=1.48$ s)

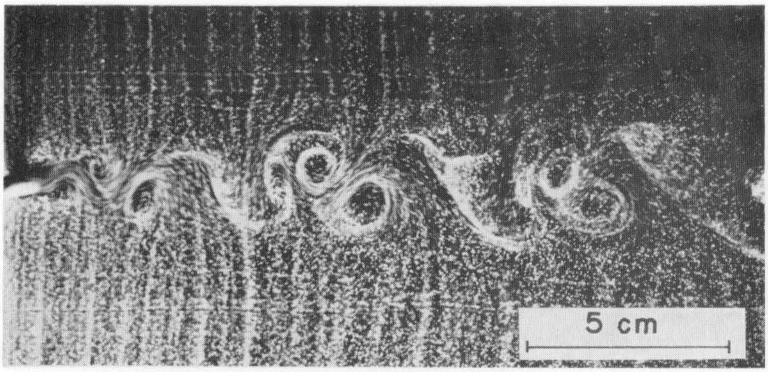

Photo. 8. Vortex wake at an upper limit of the locked-in region.
($R=100$, $A/d=0.40$, $S_c=0.217$; $U_o=2.48$ cm/s, $d=0.50$ cm, $T_c=0.93$ s)

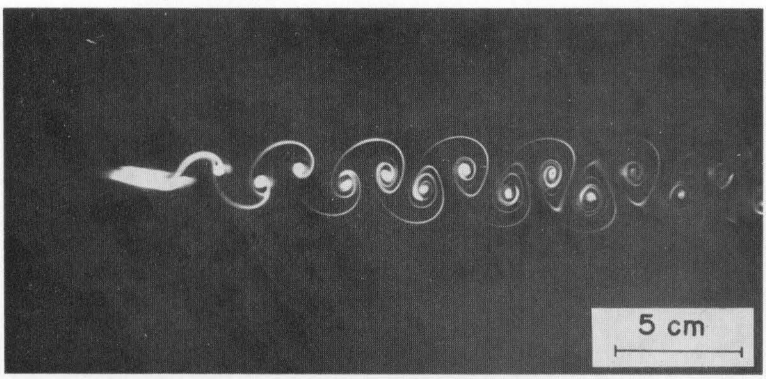

Photo. 9. Vortex wake which is locked completely. This photograph was taken by using the condensed-milk method.
($R=104$, $A/d=0.40$, $S_c=0.136$, $T_c/T_k=1.24$; $U_o=2.08$ cm/s, $d=0.50$ cm, $T_c=1.77$ s)

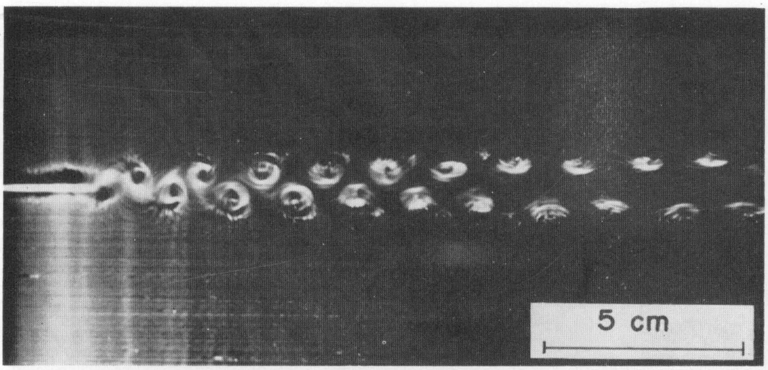

Photo. 10. Kármán vortex street behind a non-oscillating cylinder. ($R=104$, $A/d=0.67$, $S_c=0$, $S_v=0.168$; $U_o=4.45$ cm/s, $d=0.30$ cm)

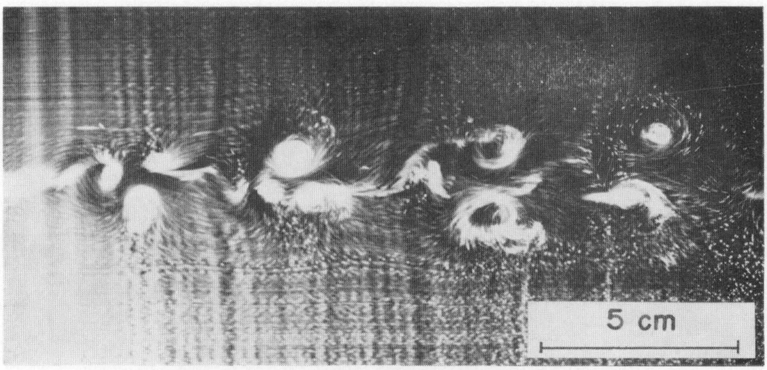

Photo. 11. Block structure of the vortex wake. ($R=104$, $A/d=0.67$, $S_c=0.098$; $U_o=4.45$ cm/s, $d=0.30$ cm $T_c=0.69$ s)

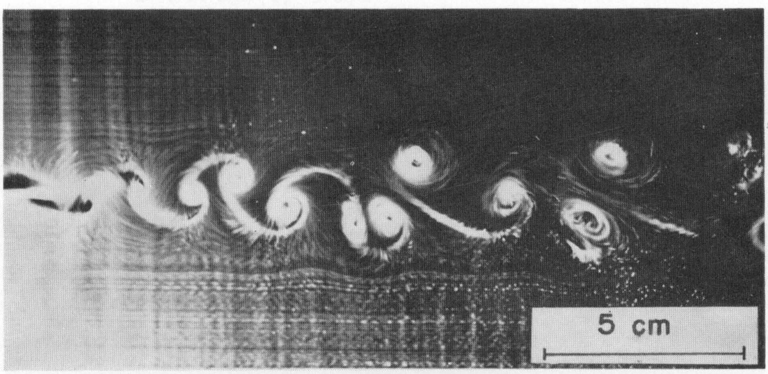

Photo. 12. Vortex wake at an incipient stage of locking-in. ($R=104$, $A/d=0.67$, $S_c=0.112$, $S_v=0.112$, $T_c/T_k=1.51$; $U_o=4.45$ cm/s, $d=0.30$ cm, $T_c=0.60$ s)

Photo. 13. Vortex wake at a large amplitude.
($R=104$, $A/d=2.28$, $S_c=0.117$, $T_c/T_K=1.44$; $U_o=1.91$ cm/s, $d=0.50$ cm, $T_c=2.24$ s)

Photo. 14. Vortex wake at a large amplitude. The lateral spacing of vortices is remarkably increased downstream.
($R=104$, $A/d=2.28$, $S_c=0.155$, $T_c/T_K=1.09$; $U_o=2.07$ cm/s, $d=0.50$ cm, $T_c=1.56$ s)

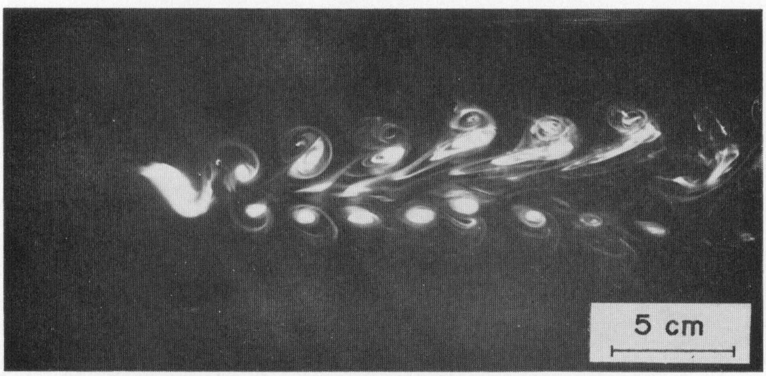

Photo. 15. Vortex wake at a large amplitude. The driving frequency is slightly higher than that for Photo. 14. The wake is still locked.
($R=104$, $A/d=2.28$, $S_c=0.179$, $T_c/T_K=0.95$; $U_o=2.07$ cm/s, $d=0.50$ cm, $T_c=1.35$ s)

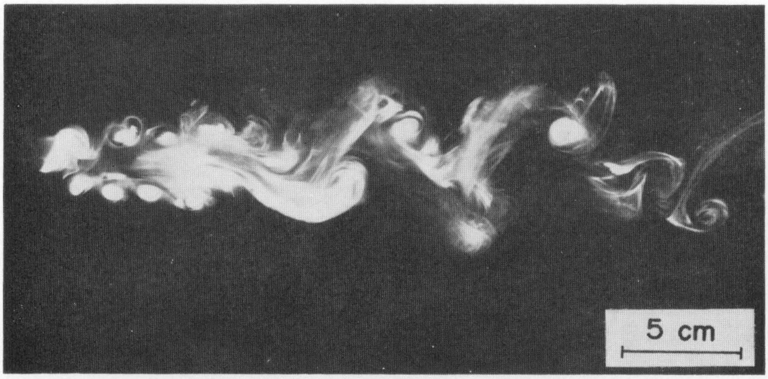

Photo. 16 Formation of the secondary Kármán vortex street. ($R=104$, $A/d=2.28$, $S_c=0.250$, $T_c/T_k=0.68$; $U_o=1.89$ cm/s, $d=0.50$ cm, $T_c=1.06$ s)

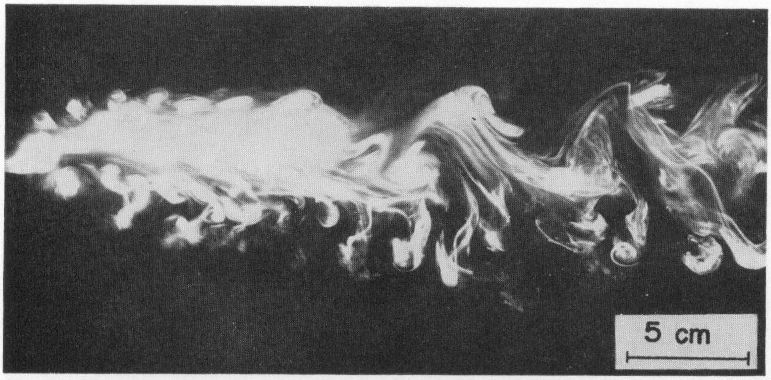

Photo. 17 Vortex wake at a large Reynolds number and a high driving frequency. ($R=163$, $A/d=1.43$, $S_c=0.394$, $T_c/T_k=0.47$; $U_o=1.85$ cm/s, $d=0.80$ cm, $T_c=1.10$ s)

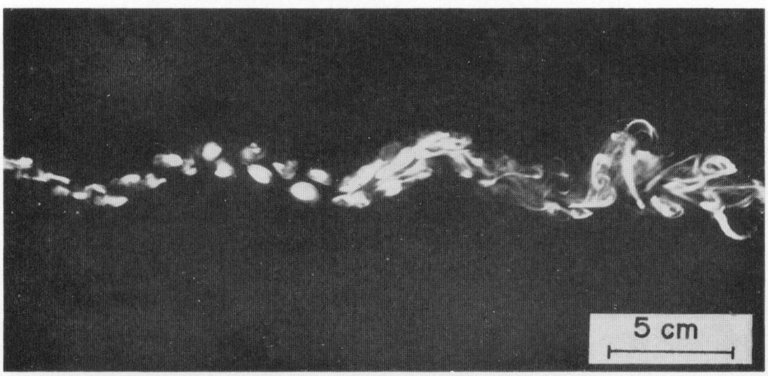

Photo. 18 Vortex wake at a large amplitude and a low driving frequency. ($R=95$, $A/d=3.80$, $S_c=0.0325$, $T_c/T_k=5.08$; $U_o=2.85$ cm/s, $d=0.30$ cm, $T_c=3.24$ s)

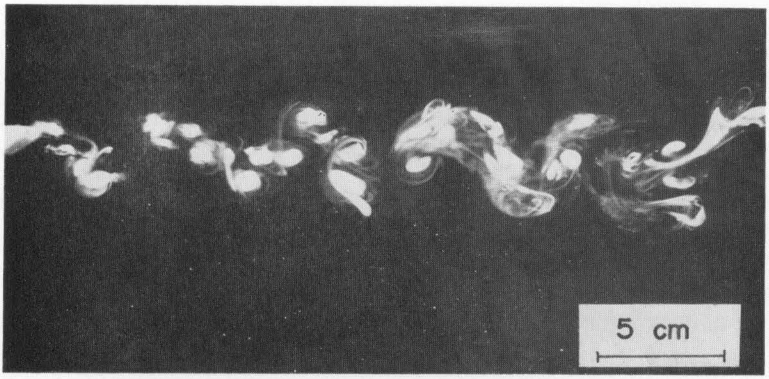

Photo. 19 Vortex wake at a driving frequency slightly higher than that for Photo. 18. ($R=95$, $A/d=3.80$, $S_c=0.049$, $T_c/T_k=3.37$; $U_o=2.85$ cm/s, $d=0.30$ cm, $T_c=2.15$ s)

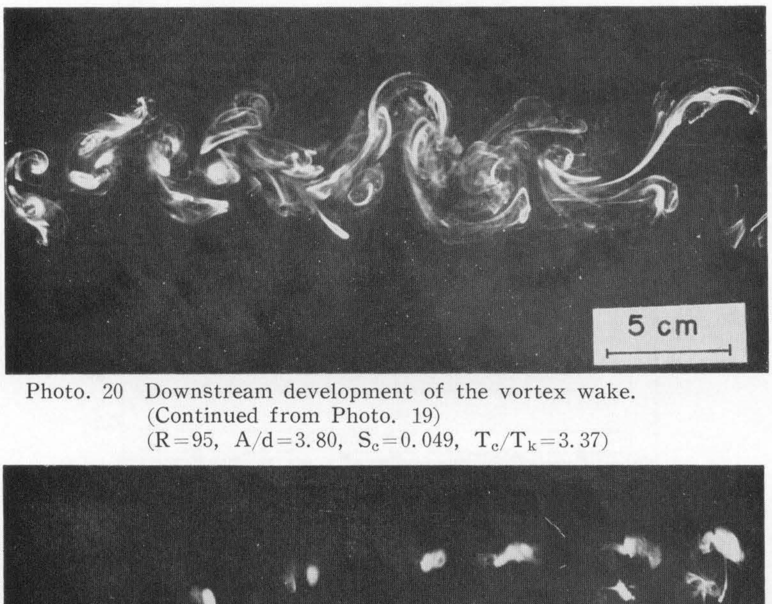

Photo. 20 Downstream development of the vortex wake. (Continued from Photo. 19)
($R=95$, $A/d=3.80$, $S_c=0.049$, $T_c/T_k=3.37$)

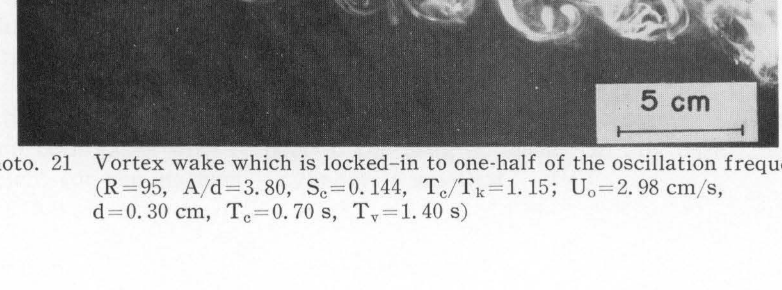

Photo. 21 Vortex wake which is locked-in to one-half of the oscillation frequency. ($R=95$, $A/d=3.80$, $S_c=0.144$, $T_c/T_k=1.15$; $U_o=2.98$ cm/s, $d=0.30$ cm, $T_c=0.70$ s, $T_v=1.40$ s)

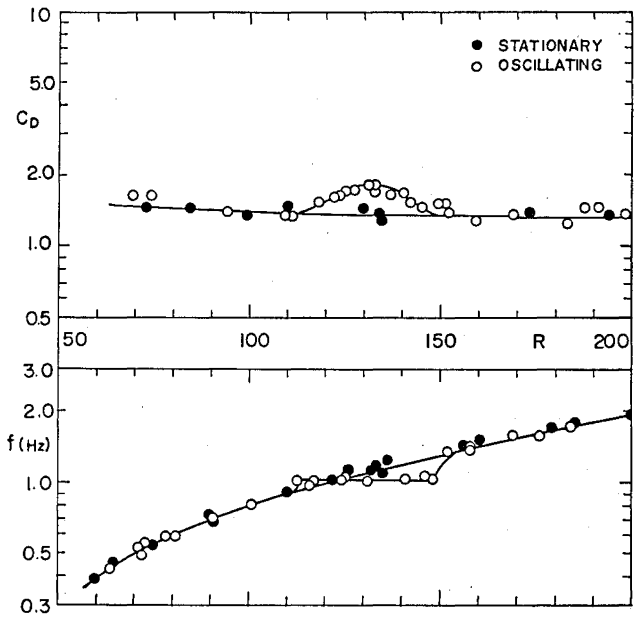

Fig. 10 C_D and f vs. R.

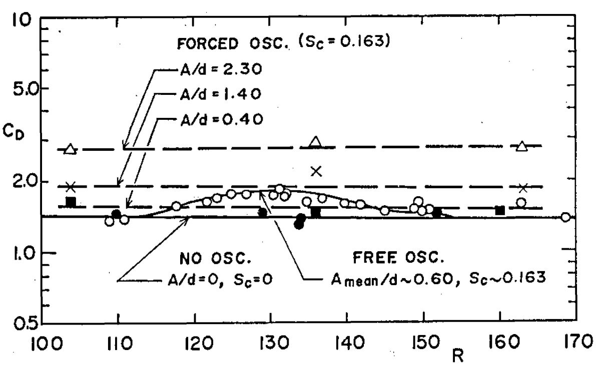

Fig. 11 Comparison of the drag coefficients.

reproduced from the previous paper [1]. The drag coefficients of the freely oscillating cylinder lie between those of the forcedly oscillating cylinder for A/d = 0.40 and for A/d = 1.40. The mean value of A/d for the freely oscillating cylinder is about 0.60. There seems to be no conspicuous difference between both cases with respect to the drag at least. In any case, the drag coefficient for the stationary cylinder is smallest.

4 Conclusion

Several quantitative measurements were carried out for the wake of the oscillating circular cylinder. For the cylinders forced to oscillate laterally, the photographs of flow patterns and the records of hot-wire signals were obtained. The relationships between the dimensionless shedding frequency and the dimensionless oscillation frequency were established at $R = 70$, 100 and 130 for the case in which the lateral displacement of the cylinder is smaller than its diameter.

Main results, which were obtained for the case where the dimensionless amplitude was less than the order of unity, are as follows. The oscillatory cylinder motion controls the vortex shedding frequency over a limited range known as the locked-in region. At the lower and the upper limits of that region, the block structure of the wake appears in the flow pattern. The phase of vortex formation is kept constant within the locked-in region. When the dimensionless amplitude is increased to the order of unity, the vortices arrange themselves in an entirely new form of the vortex street, which also is locked-in completely. For a freely oscillating circular cylinder, the locking-in of the wake also occurs. Within the locked-in region, the drag coefficient of the oscillating cylinder is always larger than that of the corresponding stationary one.

The flow past a cylinder making self-excited oscillations was not closely examined in this experiment. For a better understanding of the oscillating wake, further investigation of the effect of the oscillation amplitude on the shedding frequency seems to be necessary.

The authors would like to thank Mr. Koji Ishi-i for his collaboration through this work. Thanks are also due to the staff of Hydrodynamics Division of the Institute.

This study was supported, in part, by the Grant-in-Aid for the Scientific Research from Ministry of Education entitled "Systematic Studies of Flow Visualization".

References

1) S. Taneda and H. Honji: Rep. Res. Inst. Appl. Mech., vol. XV, No. 50, 1967, pp. 83.
2) E. Berger: Z. Flugwiss., 12 (1964) pp. 41–59.
3) O. H. Wehrmann: Phys. Fluids, 8 (1965) pp. 760–1.
4) G. K. Koopmann: J. Fluid Mech., 28 (1967) pp. 501.
5) S. Taneda: J. Phys. Soc. Japan, 20 (1965) pp. 1714–1721.
6) A. Roshko: NACA Report, 1191 (1954).
7) S. Taneda: J. Phys. Soc. Japan, 14 (1959) pp. 843–848.
8) S. Taneda: J. Phys. Soc. Japan, 18 (1963) pp. 288–296.

(Received October 17, 1968)